Chapter 5

Improving Molecular Iron Ammonia Oxidation Electrocatalysts via Substituent Tuning

.

5.1 Introduction

Ammonia oxidation (AO), and its mediation by transition metal catalysts, are burgeoning research topics across industry and academia.[1,2,3,4] Simple catalysts such as platinum and other precious metals degrade due to metal-nitride formation,[5,6] thus there is a pressing need for new catalysts that are both highly active and robust.[7,8] This motivation has inspired research into molecular AO catalysis, with the first reports appearing in 2019.[9,10,11,12] To date, a wide variety of catalyst structures have been reported, featuring ruthenium, iron, manganese, nickel, and copper catalysts with a wide variety of ligands.[13,14,15,16,17,18,19,20] Strategies such as achieving "low and level" N–H bond strengths, promoting early N–N formation to hydrazine, or enabling intermolecular nitride homocoupling all require distinct catalyst designs. As of yet, molecular AO does not feature a prevailing strategy for catalyst improvement.

Our lab has been interested in dicationic polypyridyl iron complexes $[(L_{aux})Fe(N')_2]^{2+}$ (L_{aux} = tetradentate ligand; N' = MeCN or NH_3) containing *cis*-coordination sites that bind ammonia-derived ligands (Scheme 5.1). First-generation $[(TPA)Fe(MeCN)_2]^{2+}$ featured high catalytic rates, but it was subject to degradation proceeding via displacement of the TPA ligand by excess ammonia (Eq. 1), limiting the demonstrated turnover number (TON)[21] to 16.[12] Considering the high-spin (S = 2) state of $[(TPA)Fe(NH_3)_2]^{2+}$, the primary species present during electrocatalysis, we hypothesized that degradation could be mitigated by favoring a low-spin electronic structure; indeed, use of stronger field **b**py**P**y2**M**e (BPM) led to a low-spin (S = 0) state for $[(BPM)Fe(MeCN)(NH_3)]^{2+}$ and an increased TON of 149 was demonstrated.[14]

$$[(L_{aux})Fe(NH_3)_2]^{2+} + 4\ NH_3 \rightleftharpoons L_{aux} + [Fe(NH_3)_6]^{2+} \qquad \text{(Eq. 5.1)}$$

Scheme 5.1. Molecular AO Catalysts Under Study Herein.[a]

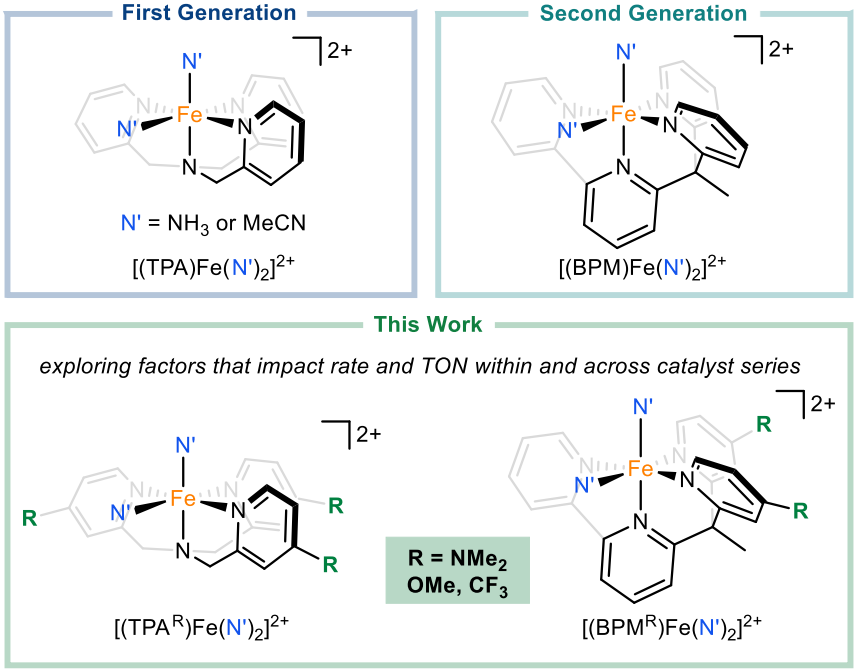

[a]Parent protio (reported) and 4-pyridyl substituted (new) complexes.

Second-generation $[(BPM)Fe(MeCN)(NH_3)]^{2+}$ also featured enhanced intrinsic catalytic rate and lowered overpotential. To rationalize this improved performance,[22,23,24,25] we consider (a) the standard potentials ($E°$) of $[(L_{aux})Fe(MeCN)_2]^{2+}$ and (b) the stability of $[(L_{aux})Fe(N')_2]^{2+}$ to demetallation. Following standard linear free energy relationships (LFER), more oxidizing complexes typically catalyze oxidative processes more rapidly, and $E°$ is greater for L_{aux} = BPM than for TPA.[26,27,28,29] In addition, demetallation of

$[(L_{aux})Fe(N')_2]^{2+}$ is reduced for L_{aux} = BPM compared to TPA, potentially increasing the concentration of active, ligated L_{aux}–Fe catalyst. In this work, we investigate these hypotheses with the goal of understanding general design principles for AO and ultimately developing an improved electrocatalyst.

5.2 Results and Discussion

To enable systematic investigation of the effect of $E°$ on catalysis, we prepared a series of 4-pyridyl-substituted auxiliary ligands and the corresponding $[(TPA^R)Fe(MeCN)_2]^{2+}$ and $[(BPM^R)Fe(MeCN)_2]^{2+}$ complexes (R = NMe_2, OMe, H, CF_3). Substitution in the 4-pyridyl position manipulates electronic structure via resonance and inductive effects without impacting the steric environment of the inner-coordination sphere. The TPA^{CF3} and substituted BPM^R ligands had not been previously synthesized. Synthetic routes analogous to the parent protio ligands furnished the trifluoromethyl derivatives but were unsuccessful for BPM^{OMe} and BPM^{NMe2}, for which we report new protocols (see SI for details).

The electronic structures of the iron complexes were quantitatively analyzed by cyclic voltametric measurement of $Fe^{2+/3+}$ redox couples (Figure 5.1). Both $[(TPA^R)Fe(MeCN)_2]^{2+}$ and $[(BPM^R)Fe(MeCN)_2]^{2+}$ exhibited reversible redox events for R = NMe_2, OMe, and H; for R = CF_3, ostensibly irreversible waves were observed. Given that the peak currents for R = CF_3 derivatives minimally change with scan number, and that reverse current is observed at more cathodic potentials (see SI), irreversibility most likely arises from a reversible change in inner-coordination sphere upon oxidation (e.g., by triflate coordination). The standard potentials were estimated using the half-wave potential ($E_{1/2}$),

except for R = CF_3, for which the half-peak potential ($E_{p/2}$) was used instead. Since half-wave and half-peak potentials for all complexes are within ±0.03 V, this approximation appears reasonable. For both $[(TPA^R)Fe(MeCN)_2]^{2+}$ and $[(BPM^R)Fe(MeCN)_2]^{2+}$, linear relationships between $E°$ and Hammett σ_p (para) values[30] were observed (see SI). The wide range of $E°$, 880 mV for TPA^R and 510 mV for BPM^R, reflects substantial variation in redox character due to 4-pyridyl substituents.

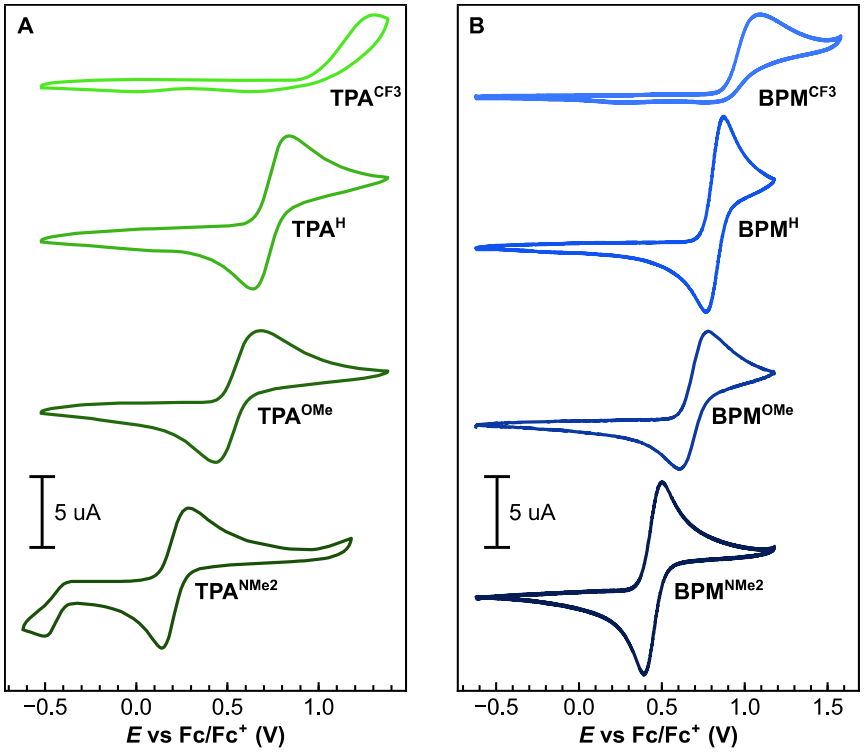

Figure 5.1. Cyclic voltammograms of (A) $[(TPA^R)Fe(MeCN)_2]^{2+}$ and (B) $[(BPM^R)Fe(MeCN)_2]^{2+}$ in acetonitrile using 0.1 M tetrabutylammonium hexafluorophosphate as supporting electrolyte at 100 mV/s with BDD WE.

To probe AO performance as a function of $E°$, we obtained cyclic voltammograms (CVs) in the presence of NH_3 (Figure 5.2A). Both $[(TPA^R)Fe(N')_2]^{2+}$ and $[(BPM^R)Fe(N')_2]^{2+}$ (N' = NH_3 or MeCN) exhibit two features in their voltammetry, E_1 and E_2, in the presence of NH_3. The lower-potential E_1 feature has been demonstrated via previous mechanistic studies

to involve net loss of a hydrogen atom from a coordinated ammine ligand (Eq. 5.2).[12,14] At the E_2 feature, these catalysts fully convert NH_3 to N_2 (Eq. 5.3).

$$E_1: \quad Fe^{II}–NH_3 + NH_3 \rightarrow Fe^{III}–NH_2 + NH_4^+ + e^- \qquad \text{(Eq. 5.2)}$$

$$E_2: \quad Fe^{III}–NH_2 + NH_3 \rightarrow Fe^{II} + N_2 + 5\ H^+ + 5\ e^- \qquad \text{(Eq. 5.3)}$$

The precatalytic wave potential (E_1) was determined using differential pulse voltammetry and analyzed as a function of $E°$ (Figure 5.2B; see SI for details). For both $[(TPA^R)Fe(N')_2]^{2+}$ and $[(BPM^R)Fe(N')_2]^{2+}$, linear correlations between E_1 and $E°$ were observed, and these correlations feature nearly identical slopes. Thus, 4-pyridyl substitution appears to exert similar influence on both catalyst series at E_1, indicating that an alteration in the first hydrogen-atom transfer in AO is not responsible for the improved performance of $[(BPM^R)Fe(N')_2]^{2+}$.

The effective turnover frequency (TOF) for the E_2 catalytic wave was similarly analyzed as a function of $E°$ (Figure 5.2C).[31] For $[(TPA^R)Fe(N')_2]^{2+}$, the datapoints are colinear. The small slope of this linear regression indicates that while $E°$ may affect AO performance within this ligand series, it does so to a very modest degree. Notably, the datapoint for $[(BPM^H)Fe(N')_2]^{2+}$ (boxed) is a clear outlier, i.e., its TOF is substantially greater than what would be predicted based upon its $E°$ value if the $[(TPA^R)Fe(N')_2]^{2+}$ regression were used. This behavior is consistent for each BPM^R complex, regardless of $E°$. However, the $[(BPM^R)Fe(N')_2]^{2+}$ series does not display an obvious correlation between TOF and $E°$, and the dataset does not indicate whether this results from an outlier versus a real trend.

However, we can disfavor the hypothesis that higher activity with $[(BPM^{H})Fe(N')_2]^{2+}$ relative to $[(TPA^{H})Fe(N')_2]^{2+}$ results primarily from greater $E°$.

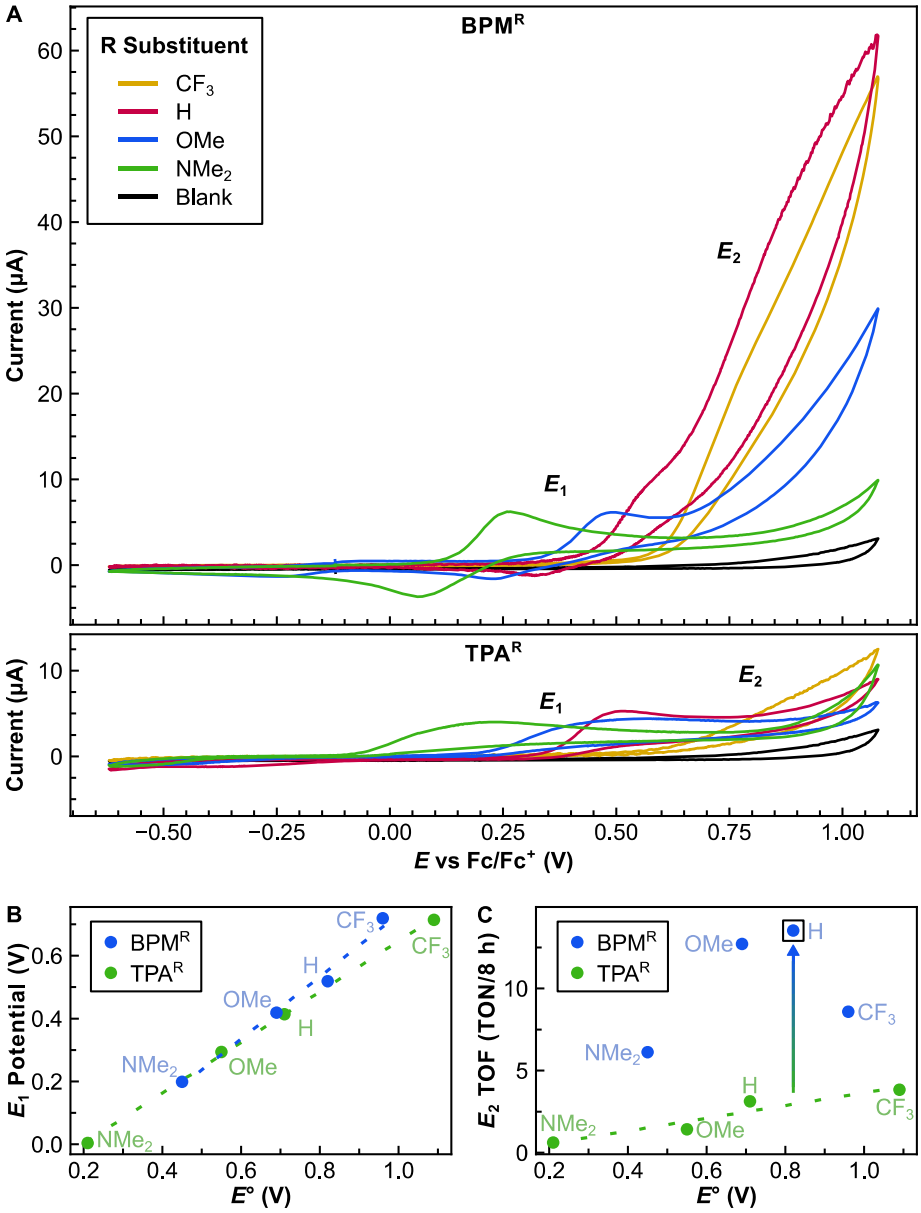

Figure 5.2. Electrochemical data. (A) Cyclic voltammograms, (B) E_1 potentials, and (C) catalytic activity at E_2 for $[(TPA^{R})Fe(N')_2]^{2+}$ and $[(BPM^{R})Fe(N')_2]^{2+}$ in acetonitrile with 50 equiv. NH_3 using 0.05 M ammonium triflate as supporting electrolyte with BDD WE.

We next studied the L_{aux} demetallation behavior of $[(L_{aux})Fe(N')_2]^{2+}$. To investigate ammonia coordination and potential displacement of L_{aux}, we titrated NH_3 into acetonitrile solutions of $[(L_{aux})Fe(MeCN)_2]^{2+}$ and monitored speciation by UV-vis spectroscopy. Following previous work, we analyzed the onset of demetallation, a metric we assign upon loss of isosbestic behavior (Figure 5.3A). The unsubstituted $[(TPA^{H})Fe(N')_2]^{2+}$ and $[(BPM^{H})Fe(N')_2]^{2+}$ AO catalysts begin to demetallate with 200 and 600 equiv. NH_3, respectively (Figure 5.3B).[12,14] The electron-withdrawing CF_3-substitutuent on both ligand scaffolds engenders substantially enhanced demetallation. By contrast, NMe_2 and OMe substituents increased the coordinating ability of the respective TPA^{R} and BPM^{R} ligands. These electron-donating groups uniformly push the measurable demetallation onset to >>2000 equivalents of NH_3. Interestingly, for L_{aux} = TPA^{NMe2} and TPA^{OMe}, stability to demetallation in the presence of ammonia is maintained despite each complex featuring of a high-spin (S = 2; see SI for details) ground state. Thus, electron-donating groups greatly reduce demetallation of catalytically relevant L_{aux}–Fe species.

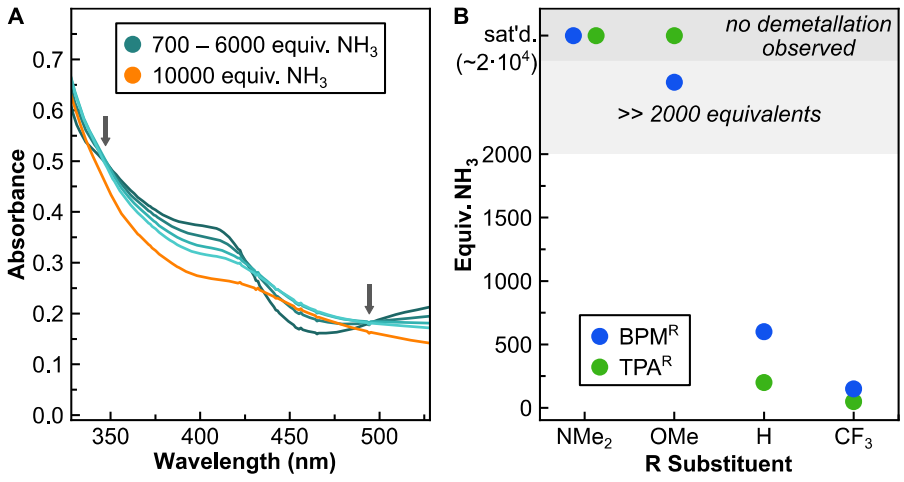

Figure 5.3. Qualitatively analyzed onset of demetallation as identified by loss of isosbestic behavior for $[(L_{aux})Fe(N')_2]^{2+}$ subjected to varying equiv. NH_3 in MeCN. (A) Example raw data for $[(BPM^{OMe})Fe(N')_2]^{2+}$ with isosbestic points marked by arrows and (B) compiled data.

By analyzing the catalysis data (Figure 5.2C) and the demetallation data (Figure 5.3) together, it is possible to rule out the hypothesis that enhanced catalysis owes to greater equilibrium catalyst concentration for $[(BPM^{H})Fe(N')_2]^{2+}$. It is important to note that our previously reported intrinsic catalytic rates ($\sim 10^7$ $M^{-1}\cdot s^{-1}$ and $\sim 10^8$ $M^{-1}\cdot s^{-1}$ for $L_{aux} = TPA^{H}$ and BPM^{H}, respectively), as well as the effective TOF data reported in Figure 2C, were obtained under ammonia concentration regimes well below the onset of demetallation. This should mitigate the influence of demetallation, if present, on catalytic rate. Three comparisons all corroborate that such a hypothesis is invalid. First, $[(TPA^{NMe2})Fe(N')_2]^{2+}$ and $[(TPA^{OMe})Fe(N')_2]^{2+}$ are both *more resistant* to demetallation but *less active* than $[(TPA^{H})Fe(N')_2]^{2+}$ or $[(TPA^{CF3})Fe(N')_2]^{2+}$. This is more readily explained as arising from the intuitive LFER between TOF and $E°$ which predicts that more oxidizing complexes operate at higher rates for oxidative processes. Second, $[(BPM^{CF3})Fe(N')_2]^{2+}$ is *less resistant* to demetallation than are $[(TPA^{R})Fe(N')_2]^{2+}$ for R = {NMe_2, OMe, or H}, but it features the *highest TOF* of these four complexes. This too could be explained by a TOF vs $E°$ LFER. However, the third comparison also invalidates any hypothesis concerning $E°$. Although $[(BPM^{NMe2})Fe(N')_2]^{2+}$ and $[(TPA^{OMe})Fe(N')_2]^{2+}$ feature *similar stability* to demetallation, and $[(TPA^{OMe})Fe(N')_2]^{2+}$ is more oxidizing than $[(BPM^{NMe2})Fe(N')_2]^{2+}$, $[(BPM^{NMe2})Fe(N')_2]^{2+}$ features a *higher TOF*. Therefore, some remaining, yet unidentified factor strongly influences catalysis.

While the aforementioned data indicate that the catalytic rate enhancement conferred by the BPM^{R} ligand scaffolds is not directly due to altered $E°$ or increased stability, increased stability is likely beneficial for achieving improved catalysis on a preparative scale, as reflected by TON. Thus, we were interested in demonstrating the practical value of these

mechanistic studies by way of improving net TON. We selected $[(BPM^{OMe})Fe(N')_2]^{2+}$ for further analysis since its TOF is minimally reduced as compared to $[(BPM^{H})Fe(N')_2]^{2+}$ (Figure 5.2C) but its stability to demetallation is substantially increased (Figure 5.3). Controlled potential coulometry data for $[(BPM^{OMe})Fe(N')_2]^{2+}$ is shown in Figure 5.4. Using the same potential as previously investigated with $[(BPM^{H})Fe(N')_2]^{2+}$ (0.85 V) allows for direct comparison. At this potential, no background electrode-mediated AO is observed.[14] In the presence of 2000 equiv. NH_3, catalytic AO proceeded for at least 48 hours, after which time 381 equiv. N_2 were measured with a quantitative faradaic efficiency (FE; within ± 5%) of 100 ± 5%. Furthermore, some catalytic activity remained after 48 hours, with a reload experiment producing 52 additional equiv. N_2. Post-catalysis, no activity is observed in a rinse test of the electrode. As $[(BPM^{H})Fe(N')_2]^{2+}$ previously demarcated the highest TON of 149 in molecular AO, this three-fold increase marks a considerable improvement. In addition to increased net activity, the higher NH_3 concentration lowered the onset potential to 0.29 V as compared to 0.45 V for $[(BPM^{H})Fe(N')_2]^{2+}$.

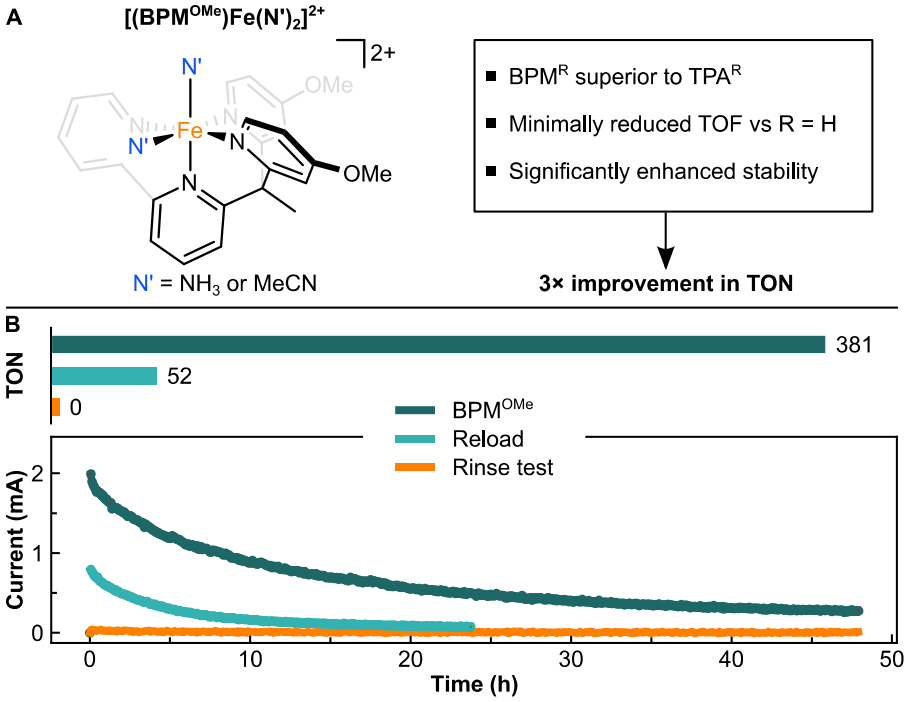

Figure 5.4. Catalyst characteristics. (A) Design elements and (B) performance of $[(BPM^{OMe})Fe(N')_2]^{2+}$. Coulometry experiments were performed with 0.05 mM [Fe] in acetonitrile with 2000 equiv. NH_3 using 0.05 M ammonium triflate as supporting electrolyte with BDD WE.

5.3 Conclusion

In conclusion, by systematically investigating $[(TPA^R)Fe(N')_2]^{2+}$ and $[(BPM^R)Fe(N')_2]^{2+}$ complexes, we have conclusively demonstrated that BPM^R ligands imbue superior performance for AO. Based on our studies of catalytic rate as a function of $E°$, we disfavor the hypothesis that enhanced catalysis in the case of R = H is solely a result of the BPM^R ligand producing a more oxidizing iron complex. Furthermore, we have validated the role of a low-spin electronic structure in mitigating demetallation but invalidated reduced demetallation as a rationale for the enhanced catalytic rate of $[(BPM^H)Fe(N')_2]^{2+}$. Nevertheless, demetallation mitigation via electron-donating substituents, as in $[(BPM^{OMe})Fe(N')_2]^{2+}$, enabled the development of a third-generation AO catalyst featuring

improved net performance as characterized by the highest TON to date. While the precise origin of enhanced catalytic rate for BPM^R ligands remains elusive, we expect that these results related to the interplay of substituent effects on activity, stability, and spin state will aid in the development of new first-row metal AO catalysts with still greater performance, as demonstrated here for $[(BPM^{OMe})Fe(N')_2]^{2+}$.

5.4 References

[1] Mandra, J. O. Yara Clean Ammonia to use Amogy's ammonia-to-power system in shipping projects. *Offshore Energy*, Novemberr 10, 2022. https://www.offshore-energy.biz/yara-clean-ammonia-to-use-amogys-ammonia-to-power-system-in-shipping-projects/.

[2] Chen, J. G.; Crooks, R. M.; Seefeldt, L. C.; Bren, K. L.; Bullock, R. M.; Darensbourg, M. Y.; Holland, P. L.; Hoffman, B.; Janik, M. J.; Jones, A. K.; Kanatzidis, M. G.; King, P.; Lancaster, K. M.; Lymar, S. V.; Pfromm, P.; Schneider, W. F.; Schrock, R. R. Beyond Fossil Fuel–Driven Nitrogen Transformations. *Science* **2018**, *360* (6391), eaar6611.

[3] MacFarlane, D. R.; Cherepanov, P. V.; Choi, J.; Suryanto, B. H. R.; Hodgetts, R. Y.; Bakker, J. M.; Ferrero Vallana, F. M.; Simonov, A. N. A Roadmap to the Ammonia Economy. *Joule* **2020**, *4* 1186–1205.

[4] Dunn, P. L.; Cook, B. J.; Johnson, S. I.; Appel, A. M.; Bullock, R. M. Oxidation of Ammonia with Molecular Complexes. *J. Am. Chem. Soc.* **2020**, *142*, 17845–17858.

[5] de Vooys, A. C. A.; Koper, M. T. M.; van Santen, R. A.; van Veen, J. A. R. The Role of Adsorbates in the Electrochemical Oxidation of Ammonia on Noble and Transition Metal Electrodes. *J. Electroanal. Chem.* **2001**, *506*, 127–137.

[6] Song, L.; Liang, Z.; Ma, Z.; Zhang, Y.; Chen, J.; Adzic, R. R.; Wang, J. X. Temperature-Dependent Kinetics and Reaction Mechanism of Ammonia Oxidation on Pt, Ir, and PtIr Alloy Catalysts. *J. Electrochem. Soc.* **2018**, *165*, J3095–J3100.

[7] Kim, H.; Hong, S.; Kim, H.; Jun, Y.; Kim, S. Y.; Ahn, S. H. Recent Progress in Pt-Based Electrocatalysts for Ammonia Oxidation Reaction. *Appl. Mat. Today* **2022**, *29*, 101640.

[8] Zhao, Y.; Setzler, B. P.; Wang, J.; Nash, J.; Wang, T.; Xu, B.; Yan, Y. An Efficient Direct Ammonia Fuel Cell for Affordable Carbon-Neutral Transportation. *Joule* **2019,** *3*, 2472–2484.

[9] Habibzadeh, F.; Miller, S. L.; Hamann, T. W.; Smith, M. R. Homogeneous Electrocatalytic Oxidation of Ammonia to N_2 Under Mild Conditions. *Proc. Natl. Acad. Sci. U.S.A.* **2019**, *116*, 2849–2853.

[10] Bhattacharya, P.; Heiden, Z. M.; Chambers, G. M.; Johnson, S. I.; Bullock, R. M.; Mock, M. T. Catalytic Ammonia Oxidation to Dinitrogen by Hydrogen Atom Abstraction. *Angew. Chem. Int. Ed.* **2019,** *58*, 11618–11624.

[11] Nakajima, K.; Toda, H.; Sakata, K.; Nishibayashi, Y. Ruthenium-Catalysed Oxidative Conversion of Ammonia into Dinitrogen. *Nat. Chem.* **2019**, *11*, 702–709.

[12] Zott, M. D.; Garrido-Barros, P.; Peters, J. C. Electrocatalytic Ammonia Oxidation Mediated by a Polypyridyl Iron Catalyst. *ACS Catal.* **2019,** *9*, 10101–10108.

[13] Dunn, P. L.; Johnson, S. I.; Kaminsky, W.; Bullock, R. M. Diversion of Catalytic C–N Bond Formation to Catalytic Oxidation of NH_3 through Modification of the Hydrogen Atom Abstractor. *J. Am. Chem. Soc.* **2020,** *142*, 3361–3365.

[14] Zott, M. D.; Peters, J. C. Enhanced Ammonia Oxidation Catalysis by a Low-Spin Iron Complex Featuring Cis Coordination Sites. *J. Am. Chem. Soc.* **2021**, *143*, 7612–7616.

[15] Trenerry, M. J.; Wallen, C. M.; Brown, T. R.; Park, S. V.; Berry, J. F. Spontaneous N_2 Formation by a Diruthenium Complex Enables Electrocatalytic and Aerobic Oxidation of Ammonia. *Nat. Chem.* **2021**, *13*, 1221–1227.

[16] Holub, J.; Vereshchuk, N.; Sánchez-Baygual, F.-J.; Gil-Sepulcre, M.; Benet-Buchholz, J.; Llobet, A. Synthesis, Structure, and Ammonia Oxidation Catalytic Activity of Ru-NH_3 Complexes Containing Multidentate Polypyridyl Ligands. *Inorg. Chem.* **2021**, *60*, 13929–13940.

[17] Toda, H.; Kuroki, K.; Kanega, R.; Kuriyama, S.; Nakajima, K.; Himeda, Y.; Sakata, K.; Nishibayashi, Y. Manganese-Catalyzed Ammonia Oxidation into Dinitrogen under Chemical or Electrochemical Conditions. *ChemPlusChem* **2021**, *86*, 1511–1516.

[18] Li, Y.; Chen, J.-Y.; Miao, Q.; Yu, X.; Feng, L.; Liao, R.-Z.; Ye, S.; Tung, C.-H.; Wang, W. A Parent Iron Amido Complex in Catalysis of Ammonia Oxidation. *J. Am. Chem. Soc.* **2022**, *144*, 4365–4375.

[19] Beiler, A. M.; Denisiuk, A.; Holub, J.; Sánchez-Baygual, F.-J.; Gil-Sepulcre, M.; Ertem, M. Z.; Moonshiram, D.; Piccioni, A.; Llobet, A. Heterogeneous Electrochemical Ammonia Oxidation with a Ru-Bda Oligomer Anchored on Graphitic Electrodes via CH–π Interactions. *ACS Energy Lett.* **2023**, *8*, 172–178.

[20] Ahmed, M. E.; Raghibi Boroujeni, M.; Ghosh, P.; Greene, C.; Kundu, S.; Bertke, J. A.; Warren, T. H. Electrocatalytic Ammonia Oxidation by a Low-Coordinate Copper Complex. *J. Am. Chem. Soc.* **2022**, *144*, 21136–21145.

[21] E_{onset} is the onset potential for catalysis, and TON is the turnover number, defined as the number of equivalents of N_2 produced per catalyst equivalent.

[22] Klug, C. M.; Cardenas, A. J. P.; Bullock, R. M.; O'Hagan, M.; Wiedner, E. S. Reversing the Tradeoff between Rate and Overpotential in Molecular Electrocatalysts for H_2 Production. *ACS Catal.* **2018**, *8*, 3286–3296.

[23] Pegis, M. L.; Wise, C. F.; Koronkiewicz, B.; Mayer, J. M. Identifying and Breaking Scaling Relations in Molecular Catalysis of Electrochemical Reactions. *J. Am. Chem. Soc.* **2017**, *139*, 11000–11003.

[24] Azcarate, I.; Costentin, C.; Robert, M.; Savéant, J.-M. Through-Space Charge Interaction Substituent Effects in Molecular Catalysis Leading to the Design of the Most Efficient Catalyst of CO_2-to-CO Electrochemical Conversion. *J. Am. Chem. Soc.* **2016**, *138*, 16639–16644.

[25] Nie, W.; Tarnopol, D. E.; McCrory, C. C. L. Enhancing a Molecular Electrocatalyst's Activity for CO_2 Reduction by Simultaneously Modulating Three Substituent Effects. *J. Am. Chem. Soc.* **2021**, *143*, 3764–3778.

[26] DuBois, D. L. Development of Molecular Electrocatalysts for Energy Storage. *Inorg. Chem.* **2014**, *53*, 3935–3960.

[27] Solomon, E. I.; Stahl, S. S. Introduction: Oxygen Reduction and Activation in Catalysis. *Chem. Rev.* **2018**, *118*, 2299–2301.

[28] Martin, D. J.; Wise, C. F.; Pegis, M. L.; Mayer, J. M. Developing Scaling Relationships for Molecular Electrocatalysis through Studies of Fe-Porphyrin-Catalyzed O_2 Reduction. *Acc. Chem. Res.* **2020**, *53*, 1056–1065.

[29] Costentin, C.; Drouet, S.; Robert, M.; Savéant, J.-M. Turnover Numbers, Turnover Frequencies, and Overpotential in Molecular Catalysis of Electrochemical Reactions. Cyclic Voltammetry and Preparative-Scale Electrolysis. *J. Am. Chem. Soc.* **2012**, *134*, 11235–11242.

[30] Hansch, Corwin.; Leo, A.; Taft, R. W. A Survey of Hammett Substituent Constants and Resonance and Field Parameters. *Chem. Rev.* **1991**, *91*, 165–195.

[31] Because of the absence of diffusion limited plateau currents, we have chosen to assess the catalytic performance at E_2 coulometrically via constant-potential experiments at E = 0.85 V vs Fc/Fc^+, as opposed to voltammetrically. While more laborious, this method proved especially important in this instance due to the presence of lower faradaic efficiencies with the derivatives bearing electron-donating groups. See the SI for additional discussion.